Rainfall over Oceans Inferred from Nimbus 7 SMMR: Application to 1982–83 El Niño

C. PRABHAKARA, D. A. SHORT, W. WISCOMBE AND R. S. FRASER

NASA/Goddard Space Flight Center, Greenbelt, MD 20771

B. E. VOLLMER

Applied Research Corporation, Landover, MD 20785

(Manuscript received 23 December 1985, in final form 17 April 1986)

ABSTRACT

Nimbus 7 Scanning Multichannel Microwave Radiometer (SMMR) measurements at five frequencies in the region 6.6 to 37 GHz, at a resolution of 155 km, are analyzed to infer precipitation over the global oceans. The microwave data show, on this spatial scale, that the combined liquid water in the clouds and rain increases the brightness temperature almost linearly with frequency in the 6.6 to 18 GHz region, while at 37 GHz such a simple relationship is not noticed. Further, as the atmospheric water vapor absorption and the effects of scattering by precipitation particles are relatively weak at 6.6 and 10.7 GHz, a technique to remotely sense the liquid water content in the atmosphere is developed based on the brightness measurements at these two frequencies. Seasonal mean patterns of liquid water content in the atmosphere derived from SMMR over global oceans relate closely to climatological patterns of precipitation. Based on this, an empirical relationship is derived to estimate precipitation over the global oceans, with an accuracy of about ±30 percent, on a seasonal basis from satellite measurements made during the three years (1979–81) before the recent El Niño event. The deviations from these three-year means, in the precipitation, produced by the 1982–83 El Niño event are then deduced from the SMMR measurements. In the Pacific one notices from these deviations that the precipitation over the ITCZ in the north, the South Pacific Convergence Zone, and the oceans around Indonesia is drastically reduced. At the same time a substantial increase in precipitation is observed over the normally dry central and eastern equatorial Pacific Ocean.

1. Introduction

Rainfall over the oceans, through the release of latent heat, can act as a source of energy to drive the circulation in the atmosphere (Gill, 1980). During El Niño/Southern Oscillation (ENSO) events the distribution of rainfall is drastically modified (Rasmusson and Wallace, 1983) as a result of complex air–sea interaction processes. For this reason, detailed observations of the anomalies of rainfall over the global oceans will be valuable to reveal the nature of such phenomena. In this study we are examining the 1982–83 ENSO event with the help of microwave satellite data.

Techniques to sense rainfall rates from passive microwave satellite measurements have been developed, among others, by Wilheit et al. (1977), Savage (1976), Wu and Weinman (1984), and Spencer et al. (1983). Basically, in these techniques the rainfall rate is related to the satellite-measured microwave brightness temperature with the help of a theoretical model. In the present study, the emphasis is placed on relating the microwave derived mean monthly or seasonal estimate of liquid water content in the atmosphere over a fairly large area, about 150 km on a side, to the mean precipitation over that area during that time.

Rainfall over the oceans is not measured satisfactorily with conventional techniques on ships. As a result, rainfall over oceans is estimated by means of indirect methods. A brief review of such methods is presented by Mintz (1981). Based on the hypothesis due to Tucker (1961), Dorman and Bourke (1979, 1981) have developed a technique to derive precipitation over oceans. This technique appears to yield a fair amount of detail and agrees fairly well with the rainfall maps derived by Rao et al. (1976) from the measurements made by the Electrically Scanning Microwave Radiometer (ESMR) carried on board Nimbus 5. ESMR had a single microwave channel at 19.3 GHz. In the present study, we are utilizing observations from the Nimbus 7 Scanning Multichannel Microwave Radiometer (SMMR), which has five channels ranging from 6.6 to 37 GHz in dual polarization.

At this time, Nimbus 7 SMMR data exists for about five years, 1979 to 1984, which includes the major El Niño event of 1982–83. We have analyzed these data to derive the three-year mean of precipitation over the oceans during non–El Niño years and deviations from the mean during the El Niño event.

Precipitation is highly variable in time and space; hence, it poses sampling problems to get satisfactory estimates (Laughlin, 1981). However, if there are helpful correlations in the spatial patterns of precipitation,

one could take advantage of that fact to mitigate this problem. In this study we are exploring such possibilities.

The satellite-based infrared techniques to sense precipitation have demonstrated their capability to get good estimates of rainfall in convectively active tropical regions (Arkin, 1983). However, in the regions away from the tropics, where cumulus convection is not dominant, such infrared derived rainfall is excessive, particularly in winter. Thus it is necessary to examine the capability of other spectral bands for improving this situation. Passive microwave measurements made by Nimbus 7 SMMR are considered in this study for this purpose.

2. SMMR information on atmospheric liquid water

SMMR has five channels in the microwave region located at 6.6, 10.7, 18, 21 and 37 GHz and measures passive emission of the atmosphere and surface in dual polarization. (For details of the instrument, see Gloersen and Hardis, 1978.) The field of view (fov) of SMMR is proportional to the wavelength of the channel. At 6.6 GHz the fov is about 155 km. The liquid water droplets in the clouds and rain produce a significant absorption in these microwave channels, and the absorption coefficient increases almost quadratically with frequency (Chang and Wilheit, 1979). This absorption has a strong dependence on the size parameter α:

$$\alpha = \pi d/\lambda \tag{1}$$

where d is the drop diameter and λ is the wavelength. Further, this absorption due to droplets has a significant negative temperature dependence. When the drops are small, i.e., $\alpha \ll 1$, as in the case of cloud drops ($d < 20$ μm), the microwave absorption in each drop is weak at these wavelengths and the absorption depends on the mass of the drops and not the size. This absorption process is said to follow the Rayleigh approximation (Gunn and East, 1954). When the absorption is weak, the negative temperature dependence is evident. However, for raindrops ($d > 500$ μm), for which the radiation properties are more accurately specified by Mie theory, absorption in each drop is strong and the effect of the temperature of the drops is rendered insignificant. To demonstrate this effect, in Table 1 the ratio of extinction at two different temperatures is shown as a function of the frequency and mean diameter of the drops. The corresponding ratio of the absorption is also listed in the table to be comprehensive. Extinction and absorption are calculated using the Mie algorithms of Wiscombe (1980) as a function of the drop size and frequency. From this table, one can notice that the temperature effect is quite vivid at long wavelengths and/or when $\alpha \ll 1$. Hence, we expect to see stronger absorption at colder temperatures, particularly at long wavelengths, for a given amount of liquid water contained in the form of light rain and cloud droplets.

TABLE 1. Variation of the ratio R [$R = e_{250}/e_{273}$] of microwave extinctions at 250 and 273 K, as a function of frequency f and mean diameter d of water drops. The corresponding ratio of the absorption for water drops is indicated within parentheses.

	d (μm)			
f (GHz)	c 9.4	g 444	h 600	i 996
6.6	2.40	1.79 (1.81)	1.37 (1.38)	0.85 (1.14)
10.7	2.12	1.50 (1.51)	1.08 (1.09)	0.89 (0.96)
18.0	2.06	1.30 (1.34)	1.05 (1.07)	1.02 (1.03)
21.0	2.00	1.25 (1.30)	1.05 (1.09)	1.04 (1.07)
37.0	1.80	1.11 (1.20)	1.02 (1.12)	1.02 (1.12)

c Cloud drop distribution C.1 of Deirmendjian (1969).
g, h, i correspond to Marshall–Palmer (1948) drop size distribution for rainfall rates of 1, 10 and 30 mm h^{-1}, respectively.

Yet another important effect in the microwave region is the scattering by hydrometeors in the form of ice particles. Wilheit et al. (1982) observed from radiometric measurements made from aircraft flying over a tropical storm over the North Atlantic that at high frequencies, 92 and 183 GHz, the scattering by precipitation-sized ice particles decreased the brightness temperature very significantly. However, at 19.3 GHz such an effect was not observed.

We have examined the SMMR data in detail as a function of frequency, geographic location, and time with the view to appreciate the temperature and ice scattering influences mentioned above. First, it was necessary to ascertain the brightness temperature of the undisturbed sea surface when there is clear weather. Brightness temperature corresponding to a calm sea surface and to clear weather is assumed to coincide with the minimum brightness temperature observed in the 6.6 GHz channel during a month at a given geographic location. The sea surface temperature map for the month, derived on the basis of this assumption, is found to agree with the ship measurements with an rms error of about 1.5°C, which bears out the validity of this assumption.

Now let us denote by T_ν° the corresponding brightness temperature at frequency ν in a given month. Let T_ν be the brightness temperature at another time during that month at the same location. Then we can define deviations as follows:

$$\delta T_\nu = T_\nu - T_\nu^\circ. \tag{2}$$

These deviations indicate the effect of either sea surface roughness produced by wind or an appreciable amount of liquid water in the atmosphere associated with rain

and clouds. This is particularly the case at 6.6 and 10.7 GHz, where the water vapor absorption is weak. However, at 18, 21 and 37 GHz, variations in the total amount of water vapor in the atmosphere can have a substantial effect on δT_ν.

At low frequencies, 6.6 and 10.7 GHz, the liquid water effect can be discriminated from that due to the surface wind effect with the help of the following ratio:

$$r = \delta T_{10.7}/\delta T_{6.6}. \quad (3)$$

From theoretical calculations (Prabhakara et al., 1983, hereafter PWCG) we find that when $r > 1.2$, the presence of liquid water is indicated. On the other hand, if $r < 1.2$, we have the surface wind effect.

In order to appreciate the relative size of the deviations δT_ν at all SMMR frequencies when $r > 1.2$, zonally averaged values of δT_ν for a month as a function of latitude were presented in PWCG. It was found that the zonal mean δT_ν in midlatitude rain belts was larger than that in the ITCZ. To illustrate this, in Fig. 1 zonal mean δT_ν, corresponding to the combined liquid water in rain and clouds during October 1979 in the North Pacific along latitudes 7.5° and 43.5°N are shown as a function of frequency. From this figure we notice that δT_ν increases linearly as a function of frequency up to about 18 GHz as the absorption is relatively weak in this region. This linearity apparently breaks down beyond 18 GHz, and δT_ν is almost a constant above 18 GHz.

The reason for this is the strong absorption by rain drops at frequencies between 18 and 37 GHz. Such absorption can reach saturation and thereby prevent further growth in brightness temperature. Also, scattering due to precipitation-sized ice particles that may be at the top levels of the rain storms can inhibit the growth in brightness temperature (Wu and Weinman, 1984). When the field of view of the instrument is large compared to the size of the rain cells these effects, between about 18 and 37 GHz, cannot be taken into account satisfactorily to relate the instrument brightness temperature measurements to rain.

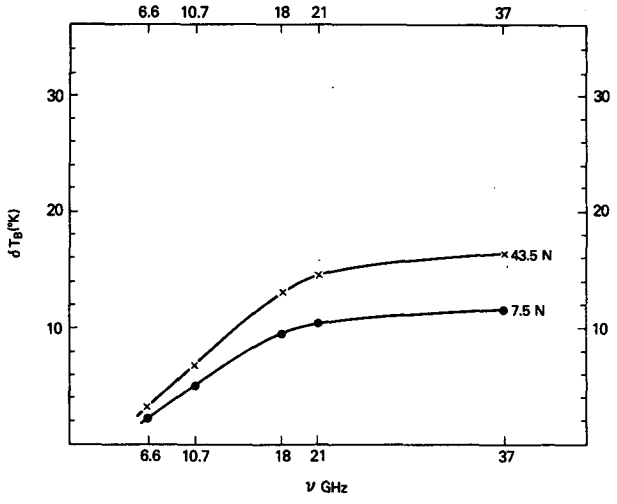

FIG. 1. Variation of zonally averaged δT_ν as a function of frequency at 7.5° and 43.5°N during October 1979.

Climatologically, we expect heavier rainfall near the ITCZ as compared to that at 43.5°N. Despite this expectation, δT_ν at all frequencies is greater at 43.5°N. Furthermore, between 6.6 and 18 GHz the slope $d\delta T/d\nu$ is larger at 43.5°N (Fig. 1). The explanation for this feature has to do with the liquid water content in the clouds that are more extensive in the midlatitudes where strong vertical wind shear associated with baroclinicity can inhibit rain (Fritsch and Chappell, 1980) and promote cloudiness. Additionally, the mean temperature of the liquid water in the clouds and light rain in the midlatitudes is colder as compared to that in the tropics. Since the emissivity is higher at lower temperatures, the brightness temperature is greater.

From the preceding discussion we deduce that when viewed with a large field of view, the 6.6, 10.7 and 18 GHz channels respond to cloud liquid water and rain in some pseudolinear fashion displaying no significant nonlinear effects due to raining cells that do not fill the "foot print" of the instrument. The response at 10.7 GHz is about one-half in magnitude as compared to that at 18 GHz. However, at 18 GHz, δT is appreciably influenced by changes in water vapor (PWCG). For this reason we have adopted the measurements at 10.7 GHz to derive the liquid water path through rain and clouds.

From theoretical calculations Tsang et al. (1977) show that the Rayleigh scattering approximation is applicable to the low frequency range, about 6 to 10 GHz, when dealing with rain drops having a mode radius of 400 μm or smaller. Following similar reasoning, in this study we are deducing the liquid water content in the clouds and rain from 6.6 and 10.7 GHz measurements. Based on theoretical simulations over the oceans, an equation to estimate liquid water content, l (g cm^{-2}), in a vertical column of the atmosphere is developed as follows (see PWCG):

$$l = \frac{20(\delta T_{10.7} - \delta T_{6.6})}{\exp[(31 - T_s)/35]} \quad (4)$$

where T_s is sea surface temperature in degrees celsius. In the numerator of Eq. (4) $\delta T_{6.6}$ is subtracted to eliminate the effect of the sea surface roughness produced by winds and rain drops.

The temperature dependence implemented in the denominator of Eq. (4) is based on the assumption that as the sea surface temperature decreases, the mean temperature of the clouds and light rain in the atmosphere also gets proportionately colder. The total liquid water content in the atmosphere derived with the help of Eq. (4) thus takes into account the gross large-scale thermal characteristics of the atmosphere.

3. Inference of precipitation

In order to infer rainfall rates from satellite-borne sensors, it would be desirable to have information on the drop size distribution and spatial variability of rain as well as the total liquid water in the rain column. In this study, SMMR measurements give us only the total liquid water in clouds and rain over a large footprint. Difficulties inherent in inferring rainfall from such limited information are elaborated in the following discussion.

Since the rain rate changes drastically in a span of a few kilometers, even the smallest field of view of SMMR, 30 km at 37 GHz channel, cannot satisfactorily resolve such detail. Further, the 37 GHz channel saturates at a relatively low rain rate of about 5 mm h^{-1}, which leads to an underestimation of the rain rate when averaged over the foot print. This is called the beam-filling problem. In estimating the rain rate from microwave techniques, assumptions regarding the drop size distribution are made. A Marshall–Palmer size distribution is commonly assumed, although that may not be applicable to all situations uniformly. The height of the rain column is parameterized in a simple fashion which may not be correct (Lovejoy, 1981). Precipitation-sized ice particles at the top of the rain column are not directly sensed by SMMR. Hence, one is forced to make some assumptions such as that the amount of these particles increases with the rain intensity (Wu and Weinman, 1984).

These assumptions are made because SMMR cannot sense these parameters. Basically, in the microwave region, information about the atmospheric liquid water present in the fov is sensed. In order to relate this information to the rain rate we must be able to separate the liquid content in the clouds from the rain satisfactorily.

From the above discussion one can see that a certain amount of empiricism and/or ad hoc assumptions are unavoidable in the rain-rate estimation schemes. The problems relating to the space and time variability and to the beam-filling may be empirically alleviated by taking advantage of certain correlations in precipitation patterns. Observations of radar echo heights, aerial extent, and the associated rain intensity made in GATE and in midlatitude regions reveal some gross correlations between these variables (Cheng and Houze, 1979). The bulk of the precipitation comes from mesoscale (50–100 km) structures. Further, as the aerial extent of the system increases, so does the duration and amount of the associated rainfall. These correlations suggest that we could relate the SMMR measured liquid water content over a 150 km scale, averaged over a time scale of about a month, to the rainfall during that period.

The emphasis is placed on the two long wavelength channels of SMMR, 6.6 and 10.7 GHz, to measure liquid water content as they have weak molecular absorption and respond linearly to liquid water. The liquid water is averaged over a month and related to rainfall.

Estimates of seasonal climatological rainfall over the oceans, based on about 20 years of ship observations, for summer and winter are given by Dorman and Bourke (1979, 1981; hereafter DB) for the Pacific and Atlantic Oceans 60°N to 30°S. Dorman and Bourke's studies discuss in detail two important problems inherent in estimating precipitation patterns over oceans. 1) Even for climatological estimates the data coverage by ships is very sparse generally south of 10°N. 2) Topographic exposure and elevation can significantly influence precipitation over islands. These factors should be taken into consideration when island stations are selected for ground truth comparison.

In our study we have developed four seasonal maps of liquid water content in the atmosphere, based on Eq. (4), over the global oceans 50°N to 50°S, utilizing the SMMR data for three years, 1979–81, prior to the recent El Niño event. These three-year mean seasonal maps could be compared with the rainfall maps of DB. Two of our mean seasonal maps, corresponding to Northern Hemisphere summer (JJA) and winter (DJF) are shown in Figs. 2a, b.

In Figs. 2a, b liquid water amounts in grams per square meter are obtained by multiplying the contour values by 10. The largest values, on the order of 240 g m^{-2}, occur near Indonesia. The largest values in the midlatitudes are about half of that, or about 120 g m^{-2}. Several features are clearly seen in these figures: the ITCZ, the South Pacific Convergence Zone (SPCZ), the convective regions along the warm water currents of the Gulf Stream and Kuroshio, and subtropical dry regions on the eastern side of the Atlantic and Pacific Oceans. These features bear a close similarity to the seasonal rainfall maps derived from ship data by DB.

In Fig. 3, climatological estimates of precipitation during northern summer along four latitudinal belts (7.5°N, 19.5°N, 31.5°N, 40.5°N) over the Pacific Ocean are compared with the SMMR sensed liquid water shown in Fig. 2b. Figure 3 shows that there is nearly a linear relationship between these two variables at low rainfall amounts. However, as the rainfall amounts get large ($\sim$1000 mm/season), as in the tropics, there is a considerable amount of scatter. Part of this scatter could be due to the poor climatology in the tropics where DB's analysis is based on a sparse amount of ship data.

From Fig. 3 we get the following empirical relationship between precipitation R (mm/season) and liquid water l (10^{-3} g cm^{-2}) measured by SMMR:

$$R = (l - 2.3)75. \quad (5)$$

This is shown as the heavy dashed line in Fig. 3. The scatter of the data shown in this figure represents a discrepancy of ±30% with respect to the mean value defined by (3).

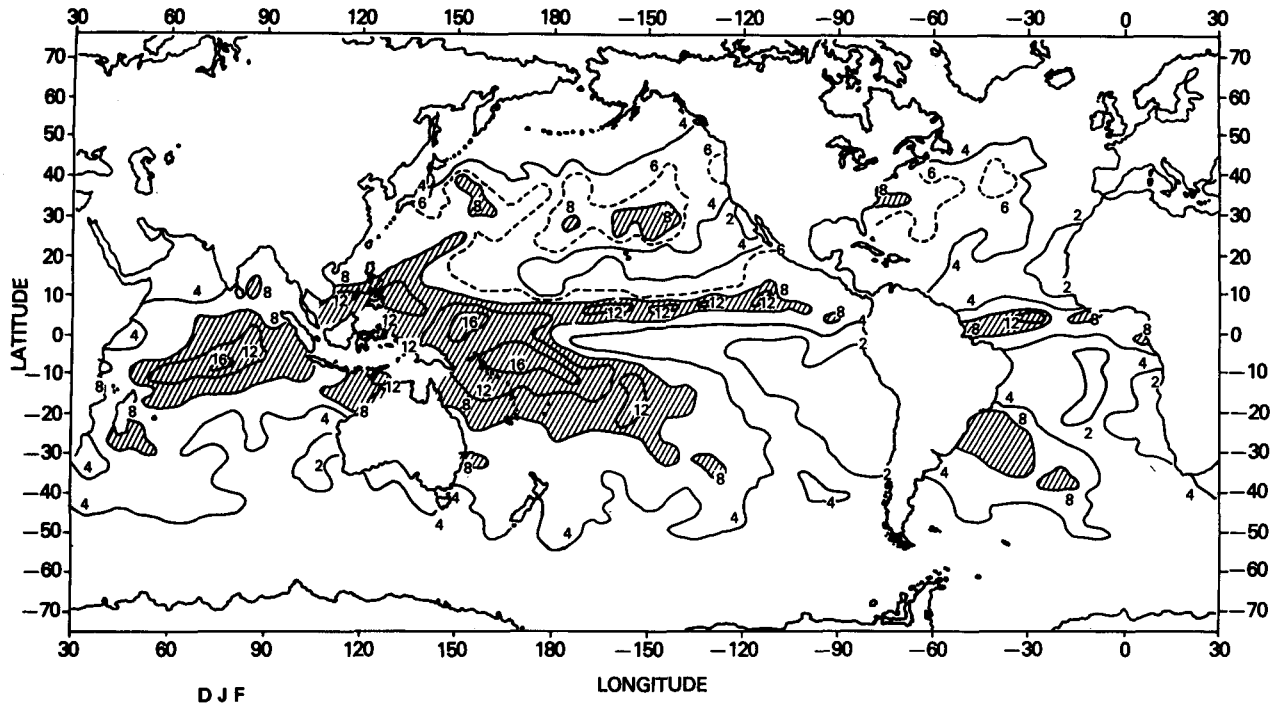

FIG. 2a. Mean liquid water content in the atmosphere (10^{-3} g cm^{-2}) during Dec, Jan and Feb, derived from SMMR data for 1979–81.

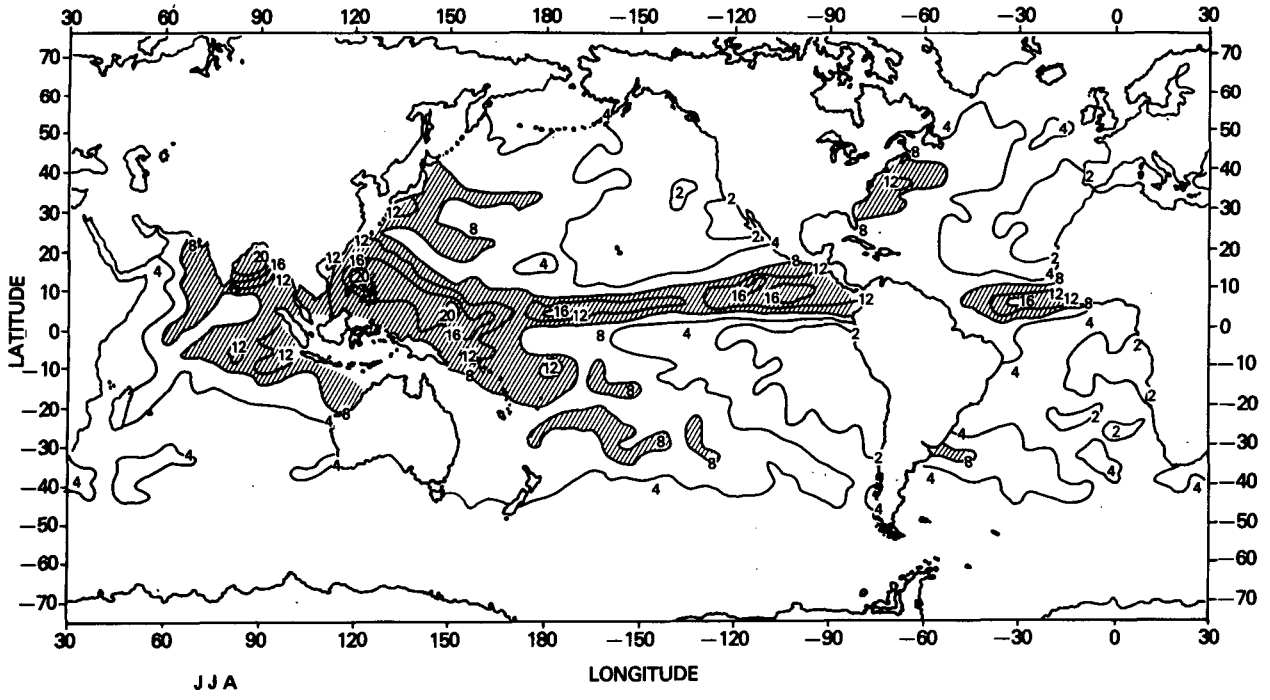

FIG. 2b. As in Fig. 2a but for Jun, Jul and Aug.

The empirical relationship between the liquid water content in the atmosphere and rainfall developed here is not inconsistent with the Marshall–Palmer (1948) equation, which relates the drop size spectrum to the rainfall intensity. Integrating with respect to drop size, the Marshall–Palmer equation yields

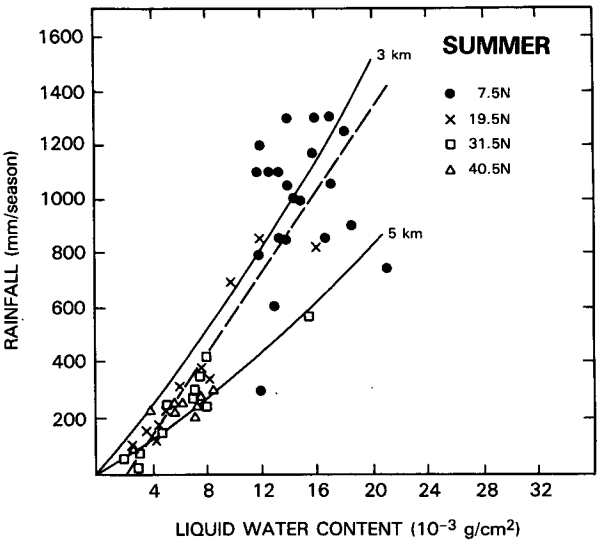

FIG. 3. SMMR derived atmospheric liquid water content (10^{-3} g cm^{-2}) vs rainfall estimates of Dorman and Bourke (1979) for summer over the North Pacific along 7.5°, 19.5°, 31.5° and 40.5° latitude belts. Heavy dashed line is an empirical fit to the data points. Thin lines are derived from Marshall–Palmer equation (see text) for rain column heights of 3 and 5 km.

$$R_{MP} = 17.8 L_{MP}^{1.19} \quad (6)$$

where R_{MP} is the rain rate (mm h^{-1}) and L_{MP} is the liquid water density (g m^{-3}) in the atmosphere. Now if we assume the height of the rain column, we can calculate R_{MP} as a function of the total liquid water content in the atmosphere. Curves obtained in this fashion for 5 and 3 km rain column heights are shown in Fig. 3. The empirical relationship adopted here approximates the curve for a 3 km rain column height.

At high latitudes, especially in winter, the depth of the liquid column decreases as the height of the freezing level decreases in the atmosphere. The SMMR sensed liquid water also decreases poleward, faster than rainfall rates inferred by DB. A substantial layer of ice particles generally lies above the liquid column in these situations, providing a source of water substance which sustains the rainfall below. Although our retrieval is not sensitive to these details, a correction to the estimated precipitation which accounts for the lower freezing level can be made by using the SMMR derived sea surface temperature. It is assumed that when the sea surface temperature drops below 18°C the clouds and rain column will begin to have some amount of these frozen particles. This frozen component increases linearly as the sea surface temperature drops. Based on these assumptions, the following equation is used to make an adjustment to the liquid water estimation until the sea surface temperature drops to 5°C:

$$l^* = [1 + (18 - T_s)/13.0]l, \quad 5°C < T_s < 18°C. \quad (7)$$

In this equation l^* is the corrected liquid water to be used in Eq. (5). Precipitation estimation is not done when the sea surface temperature drops below 5°C. The heavy dashed line in Figs. 5a, b indicates the contour of 18°C sea surface temperature, north of which the correction to the liquid estimation is made.

Island station rainfall measurements over the oceans can serve as an independent set of data to verify the relationship given by Eq. (5) that relates the SMMR derived liquid water to rainfall. For this purpose, five island stations listed in Table 2 were selected for the following reasons. These islands are small and they lie in distinct climatological regimes ranging from the ITCZ (Truk) and SPCZ (Ellice) to the transition areas between tropical and midlatitude circulation types (Rapa, Raoul, Lord Howe). From monthly mean SMMR liquid water measurements in grid boxes 3° lat × 5° long that cover each one of these islands, rainfall is estimated with the help of Eq. (5). Monthly rainfall data from island stations and SMMR are compared in the form of time series in Fig. 4. Although this is not an exhaustive comparison, it is clear that the anomalous station rainfall observed at Truk and Ellice during the most recent ENSO event (winter 1982–83) is reproduced by the SMMR inferred rainfall. This increases our confidence in interpreting spatial patterns of the rainfall anomalies to be presented in section 5. Despite the fact that on a seasonal time scale both of the datasets agree reasonably well, one can notice that there is considerable fluctuation on a monthly time scale. Because we are comparing continuous measurements at a point (station rainfall) with infrequent measurements of a related parameter over a large area (SMMR inferred rainfall), some disagreement is to be expected. This is especially the case for rainfall, a phenomenon that is highly variable in time and space. Table 2 shows the observed and the satellite-inferred average monthly rainfall for the entire observing period at each station. Reasonable agreement is obtained considering that the SMMR rainfall retrieval was developed independently of the island station observations. Also shown in Table 2 is the correlation of the monthly

TABLE 2. Comparison between monthly mean SMMR inferred rainfall vs island station measurements for the period January 1979 to October 1983.

Station	R^*	σ_{R^*}	R	σ_R	r	N
Truk (7°N)	281	153	268	198	0.54	56
Ellice (8°S)	297	137	249	172	0.53	58
Rapa (27°S)	245	145	151	133	0.37	57
Raoul (29°S)	146	107	102	116	0.35	56
Lord Howe (31°S)	123	71	87	102	0.50	58

R^* Island station measured rainfall (mm/month).
σ_{R^*} Standard deviation of monthly mean station rainfall.
R SMMR inferred rainfall (mm/month).
σ_R Standard deviation of monthly mean SMMR inferred rainfall.
r Correlation coefficient.
N Number of months.

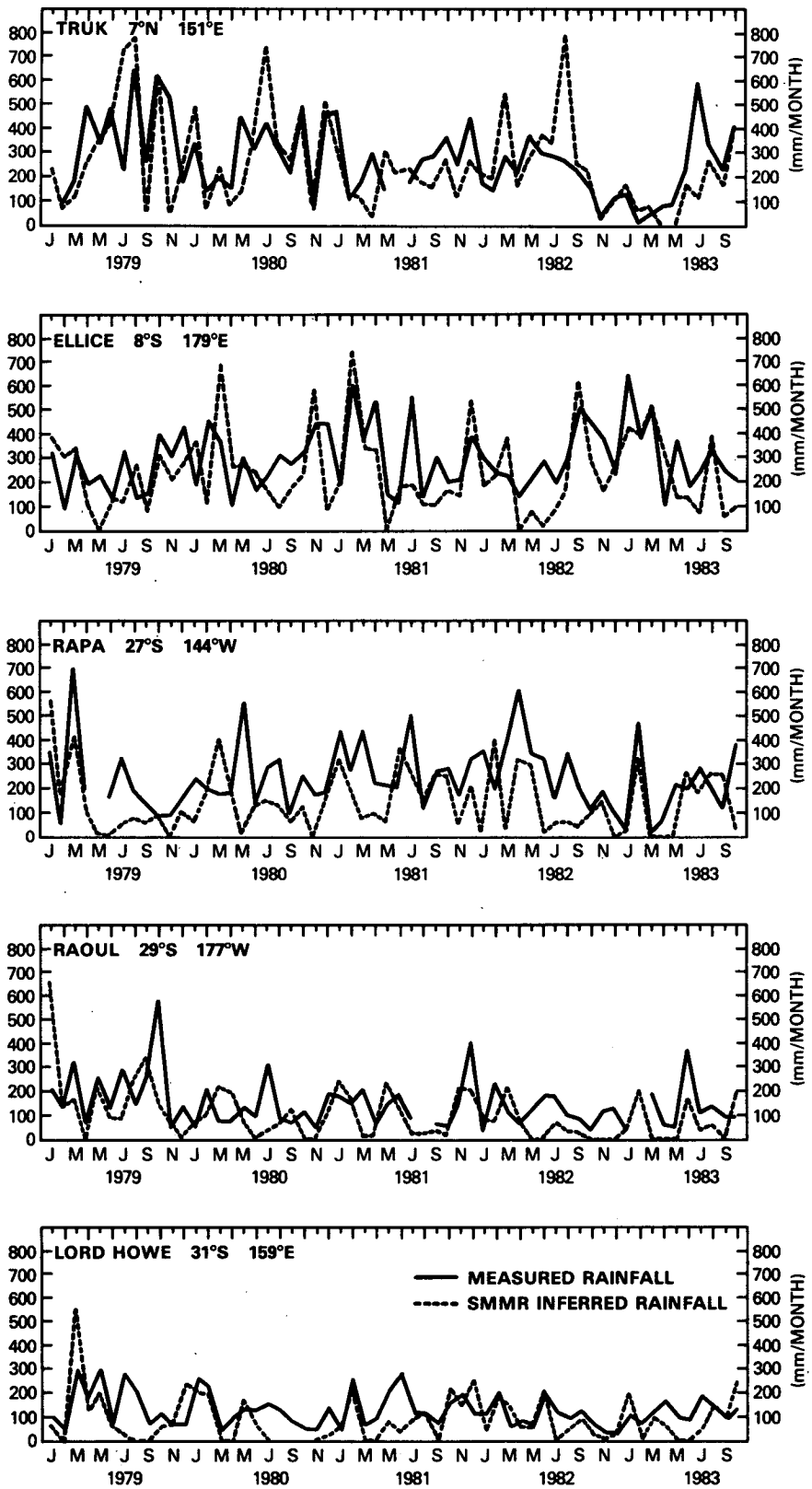

FIG. 4. Comparison between monthly mean SMMR inferred rainfall (mm) and island station measured rainfall (mm).

values for the two sets of data together with their standard deviations. Note that the standard deviation of rainfall at all stations amounts to a substantial fraction of the mean value, which emphasizes the highly variable nature of this parameter. In fact, rainfall inferred from ship-based radar reflectivity observations during GATE (GARP Atlantic Tropical Experiment; U.S. Department of Commerce, 1979) shows that despite time averaging (about three weeks for GATE phases I, II and III) rainfall totals reveal significant spatial variations within a circle of radius 200 km. This vividly illustrates one major difficulty in establishing a ground truth for space-borne precipitation measurements.

Based upon the relationships given by Eqs. (5) and (7), we have derived precipitation maps for summer (JJA) and winter (DJF) over the North and South Pacific as shown in Figs. 5a, b. These SMMR derived precipitation maps, in a gross fashion, agree with the rainfall climatology of DB. However, the precipitation at high northern latitudes, between about 45° and 50°N, is underestimated during winter despite the correction suggested in Eq. (7).

We have shown maps of precipitation derived from liquid water for the region 50°N to 30°S during winter and summer over the Pacific Ocean only. However, maps of precipitation over the global oceans for all seasons can be obtained from the corresponding liquid water maps using the linear relationship given by Eqs. (5) and (7).

We have deduced monthly mean precipitation over the oceans for about five years (1979–83), which included three years (1979–81) before the 1982–83 El Niño event. From these data we have examined seasonal and interannual variability of precipitation. It is found that where large rainfall is normally present, such as the ITCZ, SPCZ, the seas around the maritime continent, and the Bay of Bengal, the year to year variability is also large.

4. Application to the 1982–83 El Niño

Observational details pertaining to several variables such as sea surface temperature, surface winds, cloudiness, outgoing longwave radiation, and atmospheric water vapor (Rasmusson and Wallace, 1983, hereafter RW; Prabhakara et al., 1985; Ardanuy and Kyle, 1986) during different phases of El Niño events are essential to understand this complex air–sea interaction phenomenon. Precipitation inferred from SMMR over the oceans can provide additional information to understand further the nature of this phenomenon.

Seasonal mean maps of precipitation over the oceans have been derived from SMMR data obtained during the non-El Niño years 1979 to 1981. These maps represent normal conditions during quiet time. Deviations with respect to these mean maps during the 1982–83 period are derived to reveal the temporal and spatial variations produced by the El Niño event. As an example, one map of the deviations in precipitation over the oceans, constructed in the above manner from SMMR data, is shown in Fig. 6.

A significant feature in this deviation map for March–May 1983 is that in the areas over the equatorial western Pacific Ocean, where heavy precipitation is observed normally, there is a substantial deficit. At the same time, the normally dry belt associated with upwelling along the eastern equatorial Pacific and to the south of it has a large increase. In particular, from Fig. 6, we notice that the magnitude of the negative and positive anomalies are comparable. The extreme value of the negative anomaly (1100 mm) over the sea east of Indonesia amounts to almost the mean seasonal precipitation observed there during non–El Niño years. This implies a strong reversal of the mean precipitation pattern. The time series at Truk and Ellice (Fig. 4) clearly shows these effects.

The anomalous wet and dry regions inferred from infrared outgoing longwave radiation (OLR) yield a similar picture to that shown by SMMR (RW, 1983). However, the OLR inferred negative anomaly in precipitation is significantly smaller, about one-half of the postive anomaly. The SMMR inferred positive and negative anomalies are comparable. This suggests that the SMMR data can better reveal the negative anomalies in rainfall.

In order to highlight the SMMR derived precipitation anomalies, monthly mean zonal averages on the eastern Pacific from the dateline to the coastline of North and South America are plotted from January 1982 to May 1984 (Fig. 7). From this figure we notice positive anomalies start to develop along the equator from about June 1982, when the El Niño event started (RW). Apparently, the peak of activity that occurred between January and February 1983 coincides with the farthest southward migration, to about 5°S, of the precipitation in the eastern Pacific.

In essence, the SMMR observations reveal several of the spatial and temporal variations in the precipitation over the oceans produced by the 1982–83 El Niño event, such as the anomalous dry and wet regions and the development, intensification, and migration of the precipitation maximum with time toward the east.

5. Discussion and conclusions

Precipitation is a highly variable quantity. This high degree of variability suggests that we have to sample precipitation adequately in time and space. However, if there are helpful correlations in precipitation patterns in space and time we can take advantage of that. Radar observations of precipitation in GATE and in mid-latitudes suggest that the bulk of the precipitation comes from mesoscale (50–100 km) structures and that there are gross correlations among variables such as precipitation intensity, aerial extent, duration, and amount of rainfall. These correlations have been used

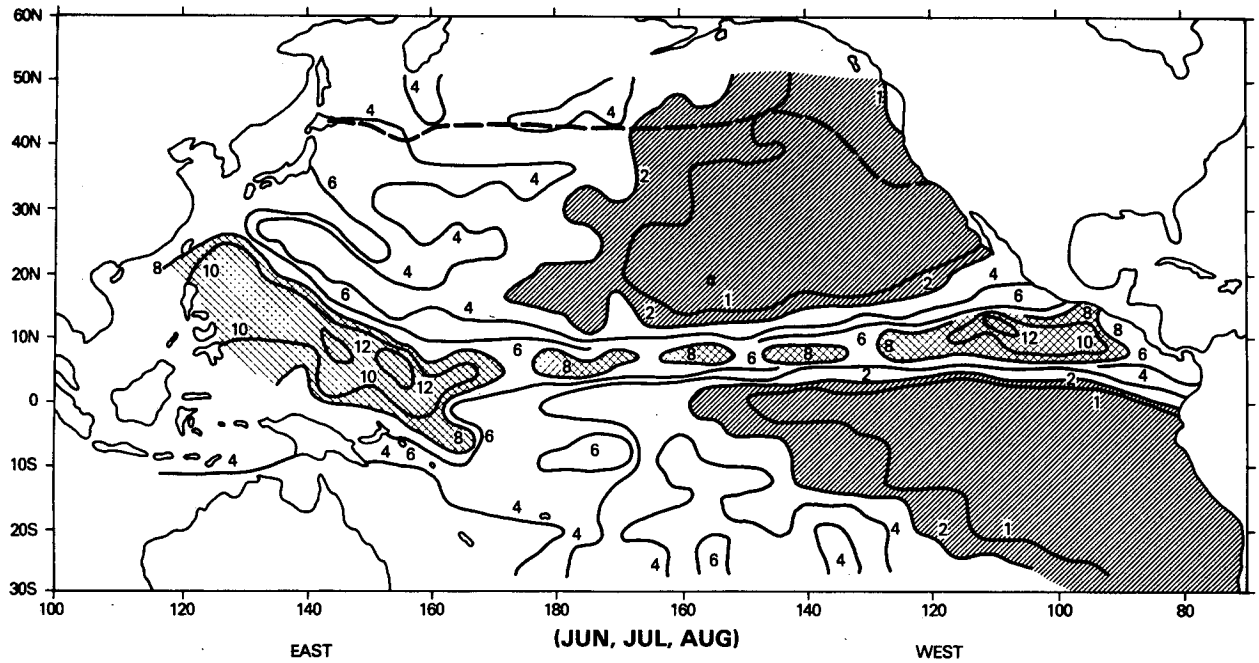

FIG. 5a. Mean SMMR inferred rainfall (10^2 mm) for Jun, Jul and Aug 1979–81 over the Pacific Ocean between 50°N and 30°S. Rainfall less than 200 mm and greater than 800 mm are identified by different shading.

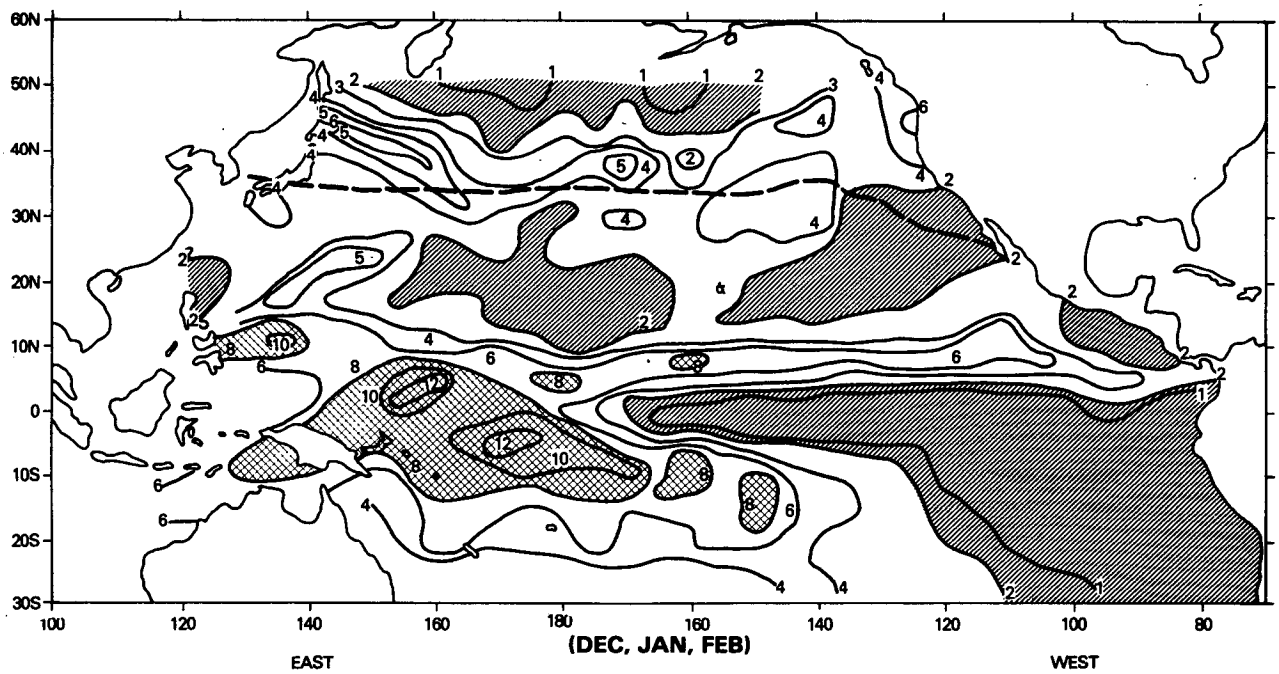

FIG. 5b. As in Fig. 5a but for Dec, Jan and Feb.

to our advantage in this study so that we could adopt a wide field of view (150 km), such as that provided by the SMMR 6.6 and 10.7 GHz channels, to obtain spatial- and time-averaged measurements of precipitation.

The beam-filling problem associated with a large field of view, when a strongly absorbing frequency such as 37 GHz is used, has been minimized in this study by choosing a weakly absorbing low frequency at 10.7 GHz.

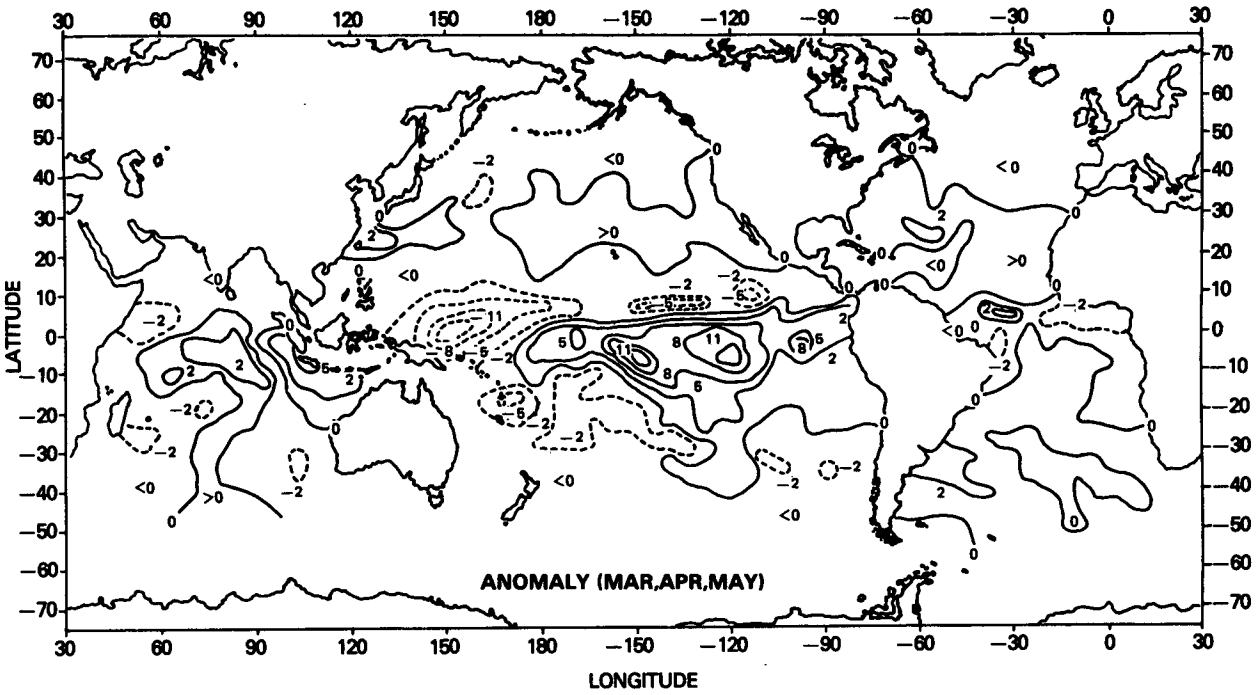

FIG. 6. Rainfall anomaly (10^2 mm) inferred from SMMR for Mar, Apr and May of 1983. Contours of negative anomalies are indicated by dashed lines.

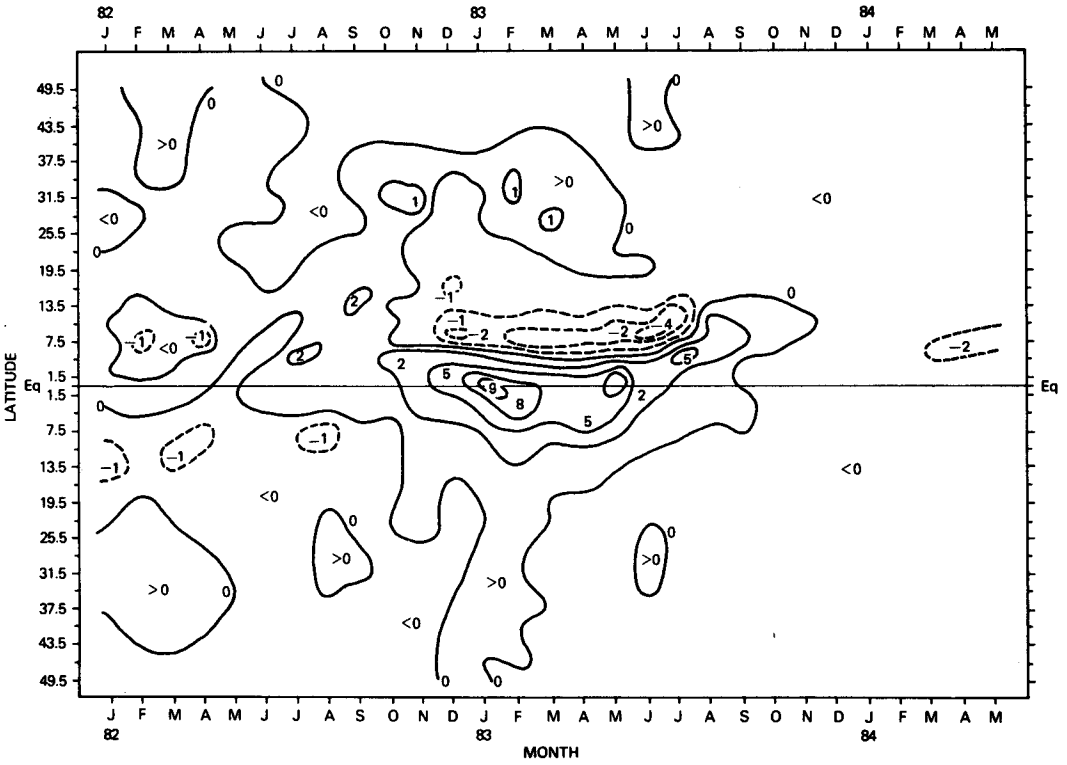

FIG. 7. Latitude–time plot of zonal mean SMMR inferred rainfall anomalies 10^2 (mm) between the dateline and the coast of North and South America.

The seasonal mean liquid water estimates over the global oceans between 50°N and 50°S show a strong similarity to the climatological maps of precipitation. This fact is used to infer precipitation from SMMR. When the SMMR estimates of monthly mean precipitation are compared with the corresponding measurements of precipitation at five island stations in the Pacific Ocean, a correlation of about 0.5 is obtained.

The seasonal mean precipitation maps over the oceans inferred from SMMR data show the usefulness of this information to global climatology and, in particular, to the studies involving El Niño and interannual variability of precipitation.

REFERENCES

Ardanuy, P. E., and H. L. Kyle, 1986: El Niño and outgoing longwave radiation: Observations from Nimbus-7 ERBS. *Mon. Wea. Rev.*, **114,** 415–433.

Arkin, P., 1983: A diagnostic precipitation index from infrared satellite imagery. *Trop. Ocean–Atmos. Newslett.*, **17,** 5–7.

Chang, A. T. C., and T. T. Wilheit, 1979: Remote sensing of atmospheric water vapor, liquid water and wind speed at the ocean surface by passive microwave techniques from Nimbus 5 satellite. *Radio Sci.*, **14,** 793–803.

Cheng, C. P., and R. A. Houze, 1979: The distribution of convective and mesoscale precipitation in GATE radar echo patterns. *Mon. Wea. Rev.*, **107,** 1370–1381.

Deirmendjian, D., 1969: *Electromagnetic Scattering on Spherical Polydispersion.* Elsevier, 78 pp.

Dorman, C. E., and R. H. Bourke, 1979: Precipitation over the Pacific Ocean, 30°S to 60°N. *Mon. Wea. Rev.*, **107,** 896–910.

——, and ——, 1981: Precipitation over the Atlantic ocean, 30°S to 70°N. *Mon. Wea. Rev.*, **109,** 554–563.

Fritsch, J. M., and C. F. Chappell, 1980: Numerical prediction of convectively driven mesoscale pressure systems. Part 1: Convective parameterization. *J. Atmos. Sci.*, **37,** 1722–1733.

Gill, A. E., 1980: Some simple solutions for heat induced tropical circulation. *Quart. J. Roy. Meteor. Soc.*, **106,** 447–462.

Gloersen, P., and L. Hardis, 1978: Scanning multichannel microwave radiometer (SMMR) experiment. *Nimbus 7 User's Guide,* C. R. Madris, Ed., NASA/GSFC, 213–245.

Gunn, L. L. S., and T. W. R. East, 1954: Microwave properties of precipitation particles. *Quart J. Roy. Meteor. Soc.*, **80,** 522–545.

Laughlin, C., 1981: On the effect of temporal sampling on the observation of mean rainfall. *Precipitation Measurements from Space—Workshop Report,* D. Atlas and O. W. Thiele, Eds., NASA/GSFC, D59–D66.

Lovejoy, S., 1981: Combining visible and infrared techniques with LAMMR for daily rainfall estimates. *Precipitation Measurements from Space—Workshop Report,* D. Atlas and O. W. Thiele, Eds., NASA/GSFC, D184–D191.

Marshall, J. S., and W. M. Palmer, 1948: The distribution of raindrops with size. *J. Meteor.*, **5,** 165–166.

Mintz, Y., 1981: A brief review of the present status of global precipitation estimates. *Precipitation Measurements from Space—Workshop Report,* D. Atlas and O. W. Thiele, Eds., NASA/GSFC, D1–D4.

Prabhakara, C., I. Wang, A. T. C. Chang and P. Gloersen, 1983: A statistical examination of Nimbus 7 SMMR data and remote sensing of sea surface temperature, liquid water content in the atmosphere and surface wind speed. *J. Climate Appl. Meteor.*, **22,** 2023–2037.

——, D. A. Short and B. E. Vollmer, 1985: El Niño and atmospheric water vapor: Observations from Nimbus 7 SMMR. *J. Climate Appl. Meteor.*, **24,** 1311–1324.

Rao, M. S. V., M. V. Abbott III and J. S. Theon, 1976: *Satellite Derived Global Oceanic Rainfall Atlas.* X-911-76-116, Goddard Space Flight Center, 31 pp and maps.

Rasmusson, E. M., and J. M. Wallace, 1983: Meteorological aspects of the El Niño/Southern Oscillation. *Science,* **222,** 1195–1202.

Savage, R. C., 1976: The transfer of thermal microwaves through hydrometeors. Ph.D. thesis, University of Wisconsin–Madison, 147 pp.

Spencer, R. W., B. B. Hinton and W. S. Olson, 1983: Nimbus 7 37 GHz radiances correlated with radar rain rates over the Gulf of Mexico. *J. Climate Appl. Meteor.*, **22,** 2095–2099.

Tsang, L., J. A. Kong, E. Njoku, D. H. Staelin and J. W. Waters, 1977: Theory for microwave thermal emission from a layer of cloud or rain. *IEEE Trans. Antennas Propag.* **AP-25** (5) 650–657.

Tucker, G. G., 1961: Precipitation over the North Atlantic Ocean. *Quart. J. Roy. Meteor. Soc.*, **87,** 147–158.

U.S. Department of Commerce, 1979: *GATE Radar Rainfall Atlas.* NOAA Special Rep., U.S. Govt. Printing Office, 155 pp. [Stock No. 003-019-00046-2.]

Wilheit, T. T., A. T. C. Chang, M. S. V. Rao, E. B. Rodgers and J. S. Theon, 1977: A satellite technique for quantitatively mapping rainfall rates over oceans. *J. Appl. Meteor.*, **16,** 551–560.

——, ——, J. L. King, E. B. Rodgers, R. A. Nieman, B. M. Krupp, A. S. Milman, J. S. Stratigos and H. Siddalingaiah, 1982: Microwave radiometric observations near 19.35, 92, and 183 GHz of precipitation in tropical storm Cora. *J. Appl. Meteor.*, **21,** 1137–1145.

Wiscombe, W., 1980: Improved Mie scattering algorithms. *Appl. Opt.*, **19,** 1505–1509.

Wu, R., and J. A. Weinman, 1984: Microwave radiances from precipitating clouds containing aspherical ice, combined phase, and liquid hydrometeors. *J. Geophys. Res.*, **89,** 7170–7178.